ACS OMEGA

Open Access



http://pubs.acs.org/journal/acsodf

Article

# Plant-Based Bioactive Phthalates Derived from *Hibiscus rosa-sinensis*: As In Vitro and In Silico Enzyme Inhibition

Farah Yasmin, Zill-i-Huma Nazli, Nusrat Shafiq,* Maryam Aslam, Yousef A. Bin Jardan, Hiba-Allah Nafidi, and Mohammed Bourhia*

Cite This: *ACS Omega* 2023, 8, 32677−32689

Read Online

ACCESS | Metrics & More | Article Recommendations | Supporting Information

**ABSTRACT:** *Hibiscus rosa-sinensis* is an attractive, ever-blossoming, and effortlessly available plant around the globe. The fabulous flowers of *H. rosa-sinensis* enjoy a significant status in folk medicine throughout the world and comprise a range of phyto constituents due to which this splendid flower owns numerous biological and pharmaceutical activities like antioxidant, antifungal, antimicrobial, anti-inflammatory, antipyretic, antidiabetic, and antifertility activity. Considering this, column chromatographic isolation of the phytoconstituents of ethyl acetate fraction of the flowers of *H. rosa-sinensis* was performed. A series of five phthalates including Di-*n*-octyl phthalate (**HR1**), ditridecyl phthalate (**HR2**), 1-allyl 2-ethyl phthalate (**HR3**), diethyl phthalate (**HR4**), and bis (6-methylheptyl) phthalate (**HR5**) were isolated. The structures of the isolated phthalates were elucidated by gas chromatography−mass spectrometry, $^{1}$H NMR, and $^{13}$C NMR. In silico and in vitro antidiabetic and antioxidant potential and DFT studies of isolated phthalates were carried out. In our study, isolated ligands were explored as potent antidiabetic as well as antioxidant agents as they exhibited good binding affinity (in in vitro and in silico experiments) against all selected protein targets. Compounds **HR1**−**HR5** showed that the binding affinity value ranged from −5.9 to −5.2 kcal/mol, −5.5 to −4.3 kcal/mol, and −5.0 to −4.1 kcal/mol for target proteins 1HNY, 2I3Y, and 5O40, respectively. Among all isolated phthalates, **HR5** can be a lead compound as it showed the best binding affinity with human pancreatic $\alpha$-amylase ($\Delta G$ = −5.9 kcal/mol) and displayed a minimum inhibition concentration ($IC_{50}$) of 11.69 $\mu$M among all phthalates. Compound **HR1** was the best docked and scored compound for inhibiting glutathione peroxidase; however, **HR2** possessed the lowest binding score of −5.0 kcal/mol, thus indicating the highest potential among isolated phthalates for inhibiting the superoxide dismutase. Furthermore, the top-ranked docked ligand−protein complex for each protein was assessed for stability of protein and complex mobility by molecular dynamics simulation using the IMOD server.

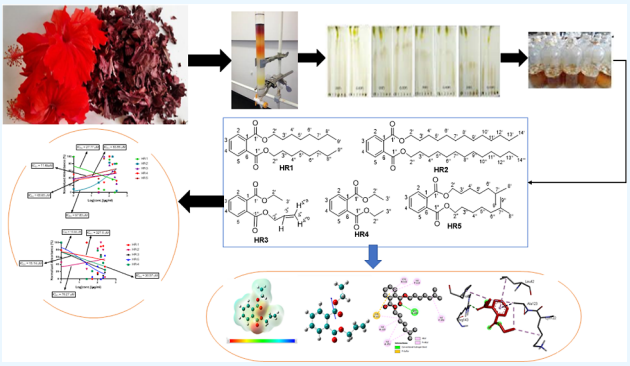


## 1. INTRODUCTION

Phthalates (phthalic acid esters) are industrial chemicals generally utilized as lubricants in plastics manufacturing. Lubricants are materials commonly mixed with other materials, particularly poly(vinyl chloride) and other polymers like styrene and rubber, to develop flexibility and elasticity in them. Phthalates are also used in food packing materials, as an adhesive for boards and plastics, paper, cellophane, aluminum foil, and paper sheets, and as a sealing material for bottles.[1] Phthalates are well-known pervasive environmental pollutants due to their extensive utilization and high tenacity in the environment.[2] Phthalates are capable of holding incredible noxious variants related to their structures in the kidneys, thyroid, liver, and testes, which are involved in general noxiousness. Moreover, they are familiar as hormonally active agents, as they can impede the human endocrine system. Occurrences of developmental irregularities (such as skeletal deformities and pronged palate, undescended testes, slashing testes weight, and anogenital gap) appear to increase through excessive exposure to phthalate metabolites.[3] Phthalates and their derivatives have been pondered as environmental contaminants due to their industrial origin. Though, this impression has altered progressively since it has been revealed that phthalates are produced by numerous organisms like plants, bacteria, and fungi, and numerous reports have validated diverse biological potentials for phthalates. Around 52 different phthalate ester derivatives have been recounted from various taxonomic groups since 1967 with a wide range of biological activities like antifungal, antibacterial, antioxidant,

Received: May 18, 2023
Accepted: August 9, 2023
Published: August 28, 2023

Table 1. Some Important Phthalates with Their Biological Activities and Sources

| S# | phthalates | source plant | activity | reference |
|---|---|---|---|---|
| 1 | diethyl phthalate | Plantago major L. | | 2 |
| 2 | di-*n*-octyl phthalate (DOP) | Plantago major L., root extract of Grewia microcos Linn. | | 2 |
| | | | | 6 |
| 3 | bis(2-ethylheptyl) phthalate | stem extract of Cynodon dactylon | anticancer, antioxidant | 1 |
| 4 | bis (2-ethylicosyl) phthalate | genus Phyllanthus | antimicrobial | 3 |
| | bis (2-ethyloctyl) phthalate | genus Phyllanthus | antimicrobial | 3 |
| 6 | di-2-ethylhexyl phtalate | flower of Calotropis gigantea | antibacterial, antifungal, anticancer | 7 |
| 7 | bis (2-methylheptyl) phthalate | leaves of Pongamia pinnata | inhibitory activity against white spot syndrome virus | 3 |

antitumor, cytotoxic, allopathic, antifouling, larvicidal, chemotactic, antiviral anti-inflammatory, and antimelanogenic activities[4] (Table 1). The continually reported biological potential of phthalates titling their valued potency can be explored for further applications other than plasticizers. To repurpose them, we checked them for their potential to use in the pharmaceutical industry.

Intensifying zest in the utilization of therapeutic plants and plant-based medications because of their emergent effects on the subsistence of human health.[5]

The isolation of pure constituents from an intact plant is a long process. Scission of a distinct constituent is very hard from complex mixtures comprising oils, fats, alkaloids, glycosides, and tannins.[8] Though by now more than 10 million secondary metabolites are identified, just a small proportion of all plant species have been investigated to a certain extent for the existence of bioactive phytoconstituents.[9] Among the approximated 4 million diverse species of plants, just 6% were found to be examined for their bioactive components and <20% were realized to be phytochemically screened. Consequently, it is highly needed to investigate the assorted bioactive fractions and the phytoanalysis and phytopharmaceutical evaluation of plant-based drugs for attaining the dreams of herbal drug discovery.[10]

The preliminary examination of therapeutic plants by chromatographic and spectrometric techniques provides fundamental data on pharmaceutical and chemical activities, which aids to choose the bioactive plants.[11]

The current research is planned to isolate the phytochemical constituents found in the therapeutic plant, *Hibiscus rosa-sinensis*, a member of the family Malvaceae.[12] *H. rosa-sinensis*, a potential and valued therapeutic plant, has been described in the primeval therapeutic literature with valuable effects in numerous health issues of humans.[13] *H. rosa-sinensis* is an attractive and ever-blossoming plant, usually familiar as a China rose. It is innate to tropical Asia and has grown in several areas of Pakistan.[14] Flowers are solitary, axillary, bell-shaped, large, and 4−6 in. in diameter with pistils and stamens projecting from the center.[15] *H. rosa-sinensis*has been recognized as a healing plant because all parts of this plant comprise numerous chemical compounds. The fabulous flowers of *H. rosa-sinensis* enjoy significant status in folk medicine throughout the world and comprises thiamine, riboflavin, citric acid, apigenidin, oxalic acid, quercetin, pelargonidin, ascorbic acid, and niacin.[16] Due to the presence of these bioactive compounds, the splendid flowers of *H. rosa-sinensis* own numerous biological and pharmaceutical activities like anti-infectious, antioxidant, antifungal, antimicrobial, anti-inflammatory, antipyretic, antidiarrheic,[13] anticonvulsants, antidiabetic, antifertility, and antihyperlipidemic activity.[17] Its therapeutic volubility has been declared in folk medications to cure a variety of ailments, e.g., all types of inflammation,[18] cough, fever, decoction given in bronchial catarrh,[19] dysentery, venereal diseases, cancerous swellings,[20] urinary infection,[19] and ulcer.[21] Juice of fresh flowers has been proven to be very beneficial to treat gonorrhea.[19] Ethanolic extract of *H. rosa-sinensis* flower possesses substantial antipyretic activity.[19] It is a widespread view that the flowers and leaves of *H. rosa-sinensis* have hair antigraying and growth-promoting characteristics.[22]

The current study emphasizes the isolation of biologically active compounds from ethyl acetate extracts of flowers of *H. rosa-sinensis* and their identification by nuclear magnetic resonance (NMR) spectroscopy and gas chromatography−mass spectrometry (GC−MS) analysis. Along with several other bioactive compounds belonging to various phytochemical groups, five phthalates were isolated and identified. Phthalates are usually used as lubricant in the plastic industry; however, we are sure that the isolated phthalates are not the contaminants of experimental procedure. In order to avoid any type of contamination, during the course of isolation and purification, we utilized the solvents of analytical grade and stored them in glass reagent bottles. So, there is no chance of introduction of these phthalates in isolation and assuredly they are from the plant itself.

The constantly reported biological potential of various phthalates such as antitumor, antiviral, anti-inflammatory, antidiabetic potential, etc., designating their valued potentiality to be reconnoitered further in dimensions other than plasticizers.

We have also assessed the efficacy of phthalates of ethyl acetate extracts of *H. rosa-sinensis* for their antidiabetic and antioxidant assay. Sequentially, in silico molecular docking and computational studies were also conducted to explore the probable role of the identified compounds as potential bioactive agents.

## 2. MATERIAL AND METHODS

**2.1. Plant Collection, Identification, and Extraction.** Fresh, healthy, dust-free *H. rosa-sinensis* (13 kg) flowers were collected from different areas of Faisalabad in July 2020 (during the flowering season), authenticated by Dr. Iqrar-ul-Hassan, taxonomist, Department of Botany, University of Agriculture, Faisalabad, where voucher specimens (numbers HRSF-103) were deposited in the herbarium. The collected flowers were dried in a shaded place for 21 days after removal of the sepals. After drying, the weight of the flowers reduced to 1.6 kg. The dried flowers were soaked in 8 L of methanol in a glass jar with an airtight lid at room temperature. The extract was filtered out after 2 weeks. The crude methanolic extract was concentrated with the help of a rotary evaporator under reduced pressure at 50 °C.[23] As a result, a reddish-brown gummy mass was obtained. The extract was suspended in


https://doi.org/10.1021/acsomega.3c03342
ACS Omega 2023, 8, 32677−32689

distilled water (1.0 L) and was fractionated into hexane (HXF) (40 g), ethyl acetate (EAF) (100 g), and methanol (MEF) (110 g) parts (Supporting Information, Scheme S1). All three fractions were concentrated with the help of a rotary evaporator under reduced pressure.

**2.2. Isolation and Purification of Compounds.** For the purification of compounds, the concentrated ethyl acetate fraction (EAF) was subjected to column chromatography to isolate pure compounds belonging to this fraction. The column chromatography was performed by packing a glass column with silica gel F254 (230−400 mesh) utilizing hexane: ethyl acetate (50:50) for making a wet packing method, and the powdery extract was loaded onto silica gel. The ascent elution technique was adopted in which the polarity of the solvent mixture was increased by the addition of ethyl acetate (50−100%) to hexane, and finally, the column was washed with methanol (Supporting Information, Figure S1).[24] 172 fractions were collected and subjected to thin-layer chromatography (TLC) for a combination of fractions having alike TLC profiles.[25]

The powdery contents of **PSHR III** were further chromatographed on a silica gel column. The elution of the column was done initially with hexane, and then, the polarity of the eluent was progressively increased by the addition of higher % age of ethyl acetate and finally the column was flushed with methanol (Supporting Information, Figure S2). Eluents were then subjected to TLC to pool the fractions with similar TLC profiles. Fractions obtained with HX/EA (80:20) gave a reddish-brown greasy compound with a single spot in TLC which we named **HR1** (Supporting Information, Figure S2). Likewise, **RSHR I** was further subjected to silica gel column chromatography using an ascent of HX: EA. The fractions eluted from the column with HX: EA (95:5 to 70:30) gave a gummy reddish-brown compound, with a single spot on TLC plate, named **HR2.** Subfractions of **RSHR I, RSHR IA**, and **RSHR IB**, gave pure compounds **HR3** and **HR4**, respectively.[26] However, elution of fraction **RSHR IB 1**(subfraction of RSHR **IB**) was obtained with HX/EA (60:40) on performing TLC gave a single spot-on TLC plate confirming the presence of the isolated and purified compound. After evaporation of the solvent, a dark brown compound was obtained which we named **HR5**.[27] Purification of compounds from different fractions was shown in systematic schemes as in Figure S3 (Supporting Information).

**2.3. Structure Elucidation of Isolated Compounds.** Isolated compounds **HR1−HR5** were characterized by $^{1}$H and $^{13}$C nuclear magnetic resonance (1H and 13C NMR) spectroscopy on Bruker 300 MHz, spectrometer, utilizing internal standards such as TMS at Quaid-e-Azam University, Islamabad, and gas chromatography−mass spectrometry (**GC−MS**) on GCMS-QP 2010 (Shimadzu, JAPAN) at Government College University, Lahore to elucidate their chemical structures.

*2.3.1. Di-n-Octyl Phthalate (**HR1**, $C_{24}H_{38}O_4$).* Reddish brown greasy compound, $^{1}$HNMR ($CDCl_3$, 300 MHz): $\delta$ 7.514 (2H, d, H-2,5), 7.34 (2H, dd, H-3,4), 3.52 (4H, t, H-2′, 2″), 1.68 (4H, t, H-3′,3″), 1.39 (4H, m, H-4′, 4″), 1.28 (12H, m, H-5′, 6′, 7′, 5″, 6″, 7″), 1.24 (4H, m, H-8′, 8″), 0.86 (6H, t, H-9′, 9″).[6] $^{13}$CNMR ($CDCl_3$, 300 MHz): 137.1 (C-1, 6), 125.8 (C-2, 5), 133.3 (C-3, 4), 167.5 (C-1′, 1″), 61.0 (C-2′,2″), 29.7 (C-3′, 3″), 24.8 (C-4′,4″), 28.3 (C-5′, 5″), 30.9 (C-6′, 6″), 32.54 (C-7′, 7″), 23.5 (C-8′, 8″), 14.1 ($2CH_3$-9′, 9″).

*2.3.2. Ditridecyl Phthalate (**HR2**, $C_{34}H_{58}O_4$).* Gummy reddish brown compound, $^{1}$HNMR (MeOD, 300 MHz): $\delta$ 7.734 (2H, d, H-2,5), 7.14 (2-H, dd, H-3,4), 3.67 (4H, t, H-2′, 2″), 1.72 (4H, m, H-3′,3″), 1.51 (4H, m, H-4′, 4″), 1.26 (4H, m, H-5′, 5″), 1.23 (28H, m, H-6′, 6″, 7′, 7″, 8′, 8″, 9′, 9″,10′, 10″, 11′, 11″, 12′, 12″), 1.23 (4H, q, H-13′, 13″), 0.76 (6H, t, H-14′, 14″). $^{13}$C NMR ($CDCl_3$, 300 MHz): $\delta$ 135.5 (C-1, 6), 126.5 (C-2, 5), 131.5 (C-3, 4), 166.7 (C-1′, 1″), 62.4 (C-2′,2″), 30.4 (C-3′, 3″), 25.3 (C-4′,4″), 28.5 (C-5′, 5″), 30.1 (C-6′, 6″,7′, 7″, 8′, 8″, 9′, 9″, 10′, 10″, 11′, 11″), 32.2 (C-12′, 12″), 21.9 (C-13′, 13″), 13.9 ($2CH_3$-14′, 14″).

*2.3.3. 1-Allyl 2-Ethyl Phthalate (**HR3**, $C_{13}H_{14}O_4$).* Reddish brown gummy compound, $^{1}$H NMR ($CDCl_3$, 300 MHz): $\delta$ 7.654 (2H, d, H-2,5), 7.36 (2H, dd, H-3,4), 3.32 (2H, q, H-2″), 3.96 (2H, d, H-2″), 1.30 (3H, t, H-3′), 5.85 (1H, m, H-3″), 5.22 (1H, d, H-4″a), 5.21 (1H, d, H-4″b). $^{13}$C NMR ($CDCl_3$, 300 MHz): $\delta$ 137.1 (C-1, 6), 125.8 (C-2, 5), 133.3 (C-3, 4), 165.7 (C-1′, 1″), 61.6 (C-2′), 14.1 (CH3−3′), 165.7 (C-1″), 66.6 (C-2″), 131.5 (C-3″), 117.5 (C-4″).

*2.3.4. Diethyl Phthalate(**HR4**, $C_{12}H_{14}O_4$).* Dark reddish-brown greasy compound, $^{1}$H NMR (MeOD, 300 MHz): $\delta$ 7.514 (2H, H-2,5), 7.34 (2H, dd, H-3,4), 4.31 (4H, q, H 2′, 2″), 1.30 (6H, t, H-3′,3″). $^{13}$C NMR (MeOD, 300 MHz): $\delta$ 137.1 (C-1, 6), 125.8 (C-2, 5), 133.3 (C-3, 4), 167.5 (C-1′, 1″), 61.0 (C-2′,2″), 14.1 ($2CH_3$-3′, 3″).

*2.3.5. Bis (6-Methylheptyl) Phthalate (**HR5**, $C_{24}H_{38}O_4$).* Dark brown gummy compound, $^{1}$H NMR (MeOD, 300 MHz): $\delta$ 7.514 (2H, d, H-2,5), 7.34 (2-H, dd, H-3,4), 3.52 (4H, t, H-2′, 2″), 1.72 (4H, m, H-3′,3″), 1.41 (4H, m, H-4′, 4″), 1.26 (4H, m, H-5′, 5″), 1.16 (4H, m, H-6′, 6″), 1.59 (2H, m, H-7′, 7″), 0.86 (12H, d H-8′, 8″, 9′, 9″). $^{13}$C NMR (MeOD, 300 MHz): $\delta$ 137.1 (C-1, 6), 125.8 (C-2, 5), 133.3 (C-3, 4), 167.5 (C-1′, 1″), 61.0 (C-2′,2″), 29.7 (C-3′, 3″), 25.8 (C-4′,4″), 25.2 (C-5′, 5″), 38.7 (C-6′, 6″), 27.7 (C-7′, 7″), 23.2 ($4CH_3$-8′, 8″, 9′, 9″).

Instrumental specifications and analysis conditions for **GC−MS** analysis are given in Table S1 (Supporting Information).

**2.4. Antioxidant (Free Radical Scavenging) Activity.** The antioxidant activities of isolated compounds (**HR1-HR5**) were assessed by utilizing diphenylpicrylhydrazyl (DPPH) as a free radical.[28] Stock solutions of purified compounds (**HR1−HR5**) with a concentration of 22 mg/mL (0.022 g) were prepared to conduct antioxidant activity. The stock solution of each compound was then diluted to desired concentrations. 4% solution of DPPH was formed by mixing 4 mg of DPPH in 100 mL of pure methanol. Ascorbic acid was utilized as a standard and prepared in water. Sample solution (1 mL) from each dilution and DPPH solution (2 mL) was added to test tubes. Similarly, ascorbic acid (1 mL) solution along with DPPH (2 mL) was added in a test tube as a control and kept undisturbed overnight. The next day, their absorbance was measured at 517 nm in triplicate utilizing a Hitachi U2900 spectrophotometer.

**2.5. Enzyme Inhibition Activity.** In vitro, the antidiabetic activity of isolated compounds (**HR1−HR5**) was assessed by utilizing starch and $\alpha$-amylase as the substrate and enzyme, respectively. Acarbose was taken as a standard drug.[5,29−31]

**2.6. Quantum Chemical Methods.** The structures of isolated phthalates were optimized through density functional theory (DFT) by 6-311G* basis set and this was carried out with B3LYP density functionals.[32] Quantum mechanically calculated descriptors augmented by DFT offer the quantitative structure−activity relationship (QSAR) for isolated compounds. DFT/B3LYP has been favored for QSAR analysis


https://doi.org/10.1021/acsomega.3c03342
ACS Omega 2023, 8, 32677−32689

and electronic and optical characteristics of compounds as this technique is organized and suggests an effectual balance among chemical precision, computational tariff, and biological activity.[31]

*2.6.1. Calculation of Micromolecular Descriptors.* Gaussian 09W was utilized to carry out all computational calculations of isolated compounds with the support of the Gauss View 6.0.16 interface to obtain an imaginal outline of optimized structures and graphical structures.[33] Hybrid type B3LYP functionals with 6311-G basis set are used for geometrical optimization of molecules in the configuration of DFT, which proposes HOMO−LUMO geometries, net charge, energy gap, dipole moment, and other structural descriptors of molecules. Quantum chemical and structural-based parameters utilizing DFT calculations to analyze SAR at DFT/B3LYP/6-311G(d) were calculated.[31]

**2.7. Molecular Docking.** *2.7.1. Protein Preparation.* The structures of selected target proteins were retrieved from protein data bank (http://www.pdb.org/pdb/home.do). Human proteins having better resolution and good ligand structure quality were selected to assess the antidiabetic and antioxidant potential of isolated ligands.[34] Moreover, target proteins were selected intentionally from different protein families to evaluate the antidiabetic and antioxidant potential of isolated phthalates at a broad spectrum level. Proteins encoding the genomic sequence of the diabetic target gene, i.e., human pancreatic $\alpha$-amylase with PDB ID: 1HNY and 1.80 Å resolution was selected. For predicting the antioxidant potential reactive oxygen species (ROS), i.e., glutathione peroxidase (PDB ID: 2I3Y, resolution: 2.00 Å) and superoxide dismutase (PDB ID: 5O40, resolution: 1.50 Å) were selected. All the heteroatoms and water molecules were detached prior to initializing the mechanism of docking.[35] Discovery Studio Visualizer v20.1. 0.19,295 (Accelrys) was utilized to attain the visualization of protein−ligand interactions.[36] Binding sites were generated using native ligand−protein interactions. Autodock Vina was utilized to transform PDB (Protein Data Bank) presentation into PDBQT [Protein Data Bank, Partial Charge (Q), and Atom Type (T)] presentation by introducing Gasteiger and Kollman charges and polar hydrogen.[37] PDBQT is the extended format of PDB which is utilized for the coordination of files. PDBQT format includes atomic partial charges, atom types, and info related to torsional degrees of freedom.[38]

*2.7.2. Ligand Preparation.* From NMR and GC−MS characterization, five phthalates were selected; their 2D structures were sketched by utilizing ChemDraw Professional 19.1.0.8; however, their 3D conformers were obtained by importing the sketched structures to Chem3D 19.1. Afterward, with the help of Open Babel, their PDB format was achieved.[39] PDB format of each ligand was converted into PDBQT format with the help of Autodock Tools 1.5.6. by introducing Gasteiger charges and polarized hydrogen and portraying the accurate bond types.[40]

*2.7.3. Scoring Function Assessment.* Molecular docking of energy-minimized 3D structures of ligands with a crystal structure of selected proteins was carried out by utilizing AutoDock tools 1.5.6. The binding affinity score was calculated based on the Lamarckian algorithm. Parameters opted for docking were as follows: population size 200, docking runs 50, and RMSD value of 2.0 Å. The binding interaction of receptor protein molecule with the best rank pose of ligand was scrutinized through binding affinity score, number of hydrogen bond interactions, and VdW interactions.[41,42]

**2.8. Molecular Dynamics Simulations.** On the base of docking outcomes, we conducted molecular dynamic simulation for the selected docked complexes (having lowest energy values) utilizing IMODS sever (http://imods.chaconlab.org)[43] with the parameters adjusted at default values.[44] IMODS is an open access web server which assists in evaluation of the stability of a complex by investigating its detailed coordinates in NMA (normal-mode analysis).[45] The all three top-ranked docked protein-ligand complexes, obtained in result of docking of phthalate ligands to the active binding pockets of proteins having PDB IDS 1HNY, 2I3Y, and 5O40 were uploaded to the IMODS server in the pdb format to assess their stability in the term of deformability plot, eigen value, *B*-factor values, covariance plots, and elastic network model.[45]

## 3. RESULTS AND DISCUSSION

**3.1. Characterization of Isolated Compounds.** The extracted purified compounds were fully characterized and identified by $^{1}$H NMR, $^{13}$C NMR, and GC−MS analysis. The spectra of the unidentified isolated compounds were compared with the spectra of the identified compounds in the library. The GC−MS spectra of the compounds were matched with the National Institute of Standards and Technology (NIST) library.

The $^{1}$H NMR data specified that compound **HR1** is a symmetrical molecule comprising a set of doublets at $\delta$ 7.154 and $\delta$ 7.34 related to aromatic protons at H-2, 5, and H-3, 4, respectively; a triplet signal at $\delta$ 3.52 ppm was distinctive of four protons of two $CH_2$ group at H-2″ and H-2″ linked to the ester; the multiplex signals at $\delta$ 1.68, 1.39, and 1.28 and 1.24 ppm were distinctive of the protons of the methylene ($CH_2$) group and the triplet signal at $\delta$ 0.86 ppm was distinctive of protons of terminal methyl ($CH_3$) group integrating for six protons.[46,47] $^{13}$C NMR confirmed the presence of six aromatic carbons at $\delta$ 137.1 for C-1, 6, $\delta$ 125.8 for C-2, 5, and $\delta$ 133.3 for C-3, 4, two ester carbonyl carbons at 167.5 ppm for C-1′, 1″, two methyl groups at $\delta$ 14.1 for C-9′, 9″ and two methylene groups attached to the oxygen of ester appeared at $\delta$ 61.0 ppm for C-2′,2″. There are 12 methylene groups at 29.7 (C-3′, 3″), 24.8 (C-4′,4″), 28.3 (C-5′, 5″), 30.9 (C-6′, 6″), 32.54 (C-7′, 7″), and 23.5 (C-8′, 8″)[1] (Supporting Information, Figure S4). The mass spectrum of compound **HR1** showed fragmental peaks at 27, 41, 57, 70, 84, 104, 132, 149, 167, and 279. Fragment peaks at 279 and 167 displayed in the mass spectrum were characteristic of alkyl phthalates and the base peak 149.0 was due to the protonated phthalic anhydride ($C_8H_5O_3$).[6] The molecular ion peak exists at 390 (Supporting Information, Figure S5). Based on the above spectral data, compound **HR1** was identified as Di-*n*-Octyl phthalate (Supporting Information, Figure S10) with the molecular formula $C_{24}H_{38}O_4$ (Mol. Weight 390).

The $^{1}$H NMR data indicated that compound **HR2** has the following kinds of protons: a set of doublets at $\delta$ 7.734 and $\delta$ 7.14 associated with aromatic protons at H-2, 5 and H-3,4, respectively; a triplet signal at $\delta$ 3.67 ppm was distinctive of four protons of two $CH_2$ groups linked to the ester at H-2″ and H-2″; the multiplex signals at $\delta$ 1.72, 1.51, 1.26, and 1.23 ppm were distinctive of the protons of the methylene ($CH_2$) group integrating for 44 protons and the triplet signal at $\delta$ 0.86 ppm was distinctive of protons of the methyl ($CH_3$) group.[48] Assignment of proton patterns was found to be similar to that


https://doi.org/10.1021/acsomega.3c03342
ACS Omega 2023, 8, 32677−32689

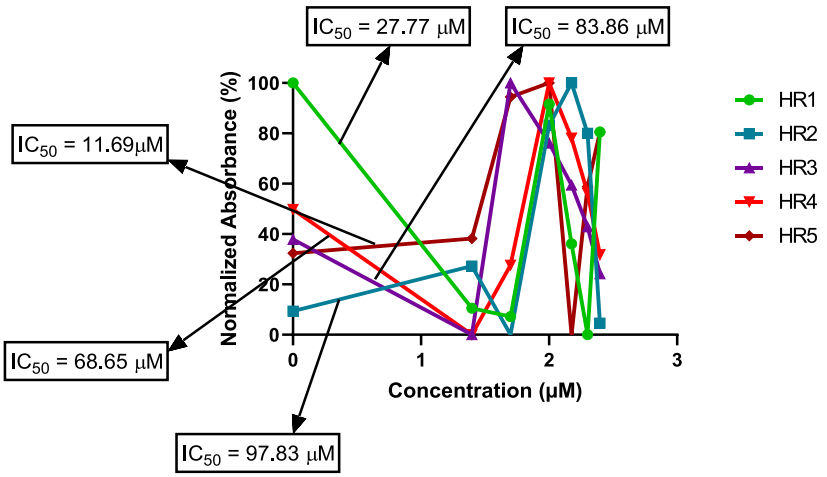


**Figure 1.** $IC_{50}$ values for antidiabetic activities.

of **HR1** with small differences. The $^{13}C$ NMR confirmed the presence of six aromatic carbons at $\delta$ 135.5 for C-1, 6, $\delta$ 126.5 for C-2, 5, and 131.5 (C-3, 4), two carbonyl carbons at $\delta$ 166.7 ppm for C-1′, 1″, two methyl groups at C-14′, 14″ appeared at $\delta$ 13.9, and two methylene groups attached to the oxygen of the ester at $\delta$ 62.4 ppm for C-2′,2″. There are 22 methylene groups at $\delta$ 30.4 (C-3′, 3″), 25.3 (C-4′,4″), and 30.1 (C-5′, 5″, 6′, 6″, 7′, 7″, 8′, 8″, 9′, 9″, 10′, 10″, 11′, 11″, 12′, 12″, 13′, 13″) and this was difference from **HR1**[48] (Supporting Information, Figure S4). Mass spectrum of compound **HR2** showed fragment peaks at 27, 41, 43, 57, 71, 85, 113, 149, 167, 168, and 335. Molecular ion peaks at 530 and fragment ion peak at 167 displayed in the mass spectrum were characteristic of alkyl phthalates, and the base peak of 149.0 was due to the protonated phthalic anhydride ($C_8H_5O_3$)[49] (Supporting Information, Figure S6). Based on the above spectral data, compound **HR2** was identified as tridecyl ester phthalate (Supporting Information, Figure S10) with the molecular formula of $C_{34}H_{58}O_4$ (Mol. Weight 530).

The $^1H$ NMR data indicated that compound **HR3** possesses the following kinds of protons: a set of doublets at $\delta$ 7.654 and $\delta$ 7.36 associated with aromatic protons at H-2, 5, and H-3, 4, respectively; a quadrat signal at $\delta$ 3.32 ppm was distinctive of two protons of a $CH_2$ group associated with ester at H-2′; a duplet signal at $\delta$ 3.96 ppm was distinctive of a $CH_2$ group associated with ester at H-2″; and a triplet signal at $\delta$ 1.30 was characteristic of the protons of a methyl group at 3′. Three multiplet signals at $\boldsymbol{\delta}$ 5.85, $\delta$ 5.22, and $\delta$ 5.21 for protons at position 3″, 4″a, and 4″b, respectively, are the representatives of protons of the allylic unsaturated group.[50] The $^{13}C$ NMR spectra exhibited 10 signals with the above-stated chemical shift values. The $^{13}C$ NMR spectral pattern exhibited three signals for six aromatic carbons at $\delta$ 137.1, 125.8, and 133.3 for (C-1, 6), (C-2, 5), and (C-3, 4), respectively, one signal at 165.7 ppm for two carbonyl carbons at position 1″ and 1″, one signal at 61.6 ppm for $CH_2$ attached to the oxygen of the ester at position 2″ and one peak at 66.6 ppm for O-bearing $CH_2$ at position 2″, one signal for methyl group of position 3′ at $\delta$14.1, one signal for C-3″ at 131.5 ppm is the clear indication of the presence of unsaturation[50] (Supporting Information, Figure S4). One signal for terminal carbon ($CH_2$) of position 4″ at 117.5 ppm. $^{13}C$ NMR spectral data of HR3 support the $^1H$ NMR spectral data. The mass spectrum of compound **HR3** presented a molecular peak at 234 and fragment ion peaks at 27, 41, 50, 65, 76, 93, 104, 121, 132, 149, 154, 177, and 188. The base peak at 149.0° was due to the protonated phthalic anhydride ($C_8H_5O_3$). The molecular ion peak exists at 390 nm (Supporting Information, Figure S7). Based on the above spectral data, compound **HR3** was identified as 1-Allyl 2-ethyl phthalate (Supporting Information, Figure S10) with the molecular formula of $C_{13}H_{14}O_4$ (Mol. Weight 234).

The $^1H$ and $^{13}C$ NMR data of **HR4** were found to be the same as those for compounds **HR1** and **HR2** having the following kinds of protons: a set of doublets at $\delta$ 7.514 and $\delta$ 7.34 associated with aromatic protons at H-5 and H-3, 4, respectively; a quadrat signal at $\delta$ 4.31 ppm was distinctive of four protons of two $CH_2$ groups attached to an ester at H-2″ and H-2″; the triplet signal at $\delta$ 0.86 ppm was characteristic of protons of the methyl ($CH_3$) group integrating for six protons while a chain of $CH_2$ was missed.[51] The $^{13}C$ NMR confirmed the presence of six aromatic carbons which gave three signals at $\delta$ 137.1 for C-1, 6, $\delta$ 125.8 for C-2, 5 and $\delta$ 133.3 (C-3, 4), two carbonyl carbons gave a characteristic peak at 167.5 ppm for C-1′, 1″, and two methylene groups linked to oxygen of ester at 61.0 ppm for C-2′,2″ and two methyl groups at C-14′, 14″ appeared at $\delta$ 14.1[52] (Supporting Information, Figure S4). The mass spectrum of compound **HR4** presented a molecular peak at 222 and fragment peaks at 27, 50, 65, 76, 93, 105, 121, 132, 149, 164, 177, and 194.[53,54] The base peak at 149.0 was due to the protonated phthalic anhydride ($C_8H_5O_3$)[6] (Supporting Information, Figure S8). Based on the above spectral data, compound **HR4** was identified as diethyl phthalate (Supporting Information, Figure S10) with the molecular formula $C_{12}H_{14}O_4$ (Mol. Weight 222).

$^1H$ NMR of compound **HR5** showed that the under-consideration compound is a symmetrical molecule that comprises four terminal methyl groups 8′, 8″, 9″, and 9″ appearing at $\delta$ 0.86 integrating for 12 protons. The aromatic protons of H-2,5 and H-3,4 appeared at $\delta$ 7.154 and 7.34, respectively. The methylene protons at 2′, 2″ attached to the ester appeared at $\delta$ 3.52 as a triplet. The other methylene protons of position H-3′,3″, H-4′, 4″, H-5′, 5″, and H-6′, 6″ appeared as multiplets at $\delta$ 1.72, 1.41, 1.26, and 1.16, respectively. However, two methine protons of positions 7 and 7″ appeared as a multiplet at $\delta$ 1.59.[47] The $^{13}C$ NMR spectrum of **HR5** supported proton NMR data. Six aromatic carbons gave three signals at $\delta$ 137.3 for C-1, 6, $\delta$ 125.8 for C-2, 5 and $\delta$ 133.3 for (C-3, 4). The ester carbonyls (C-1′, 1″)


https://doi.org/10.1021/acsomega.3c03342
ACS Omega 2023, 8, 32677−32689

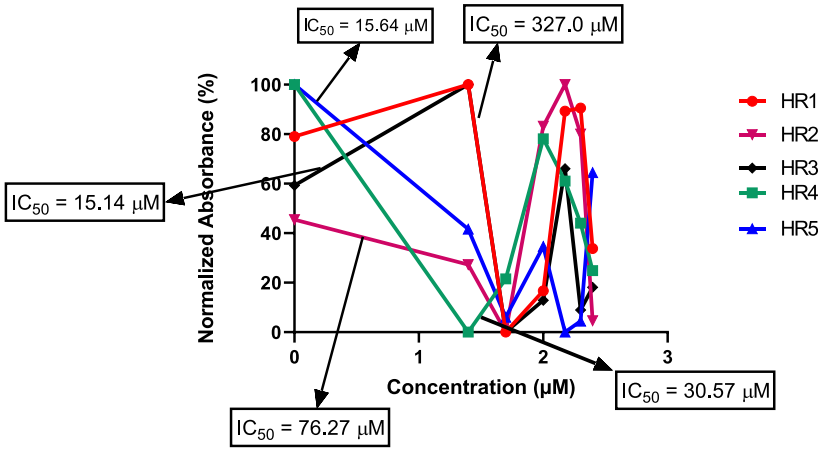


**Figure 2.** $IC_{50}$ values for antioxidant activities.

**Table 2. Quantum Chemical Parameters Were Based Upon DFT Computations for SAR Studies at DFT/B3LYP/3-21G**

| | structure−activity relationship | | | | |
|---|---|---|---|---|---|
| parameters | HR1 | HR2 | HR3 | HR4 | HR5 |
| $E_{HOMO}$ (eV) | −0.2677 | −0.2568 | −0.2674 | −0.2672 | −0.2677 |
| $E_{LUMO}$ (eV) | −0.0617 | −0.0592 | −0.0707 | −0.0694 | −0.0694 |
| energy gap "$\Delta E = E_{LUMO} - E_{HOMO}$ (eV)" | 0.20591 | 0.19765 | 0.19721 | 0.19785 | 0.19827 |
| dipole moment "$\mu$(Debye)" | 0.569455 | 3.054507 | 3.682993 | 3.454246 | 3.589851 |
| chemical hardness "$\eta$ (eV) | 0.1029 | 0.0988 | 0.0983 | 0.0989 | 0.0991 |
| chemical softness "S" | 4.857 | 5.059 | 5.084 | 5.055 | 5.044 |
| electronegativity "$\chi$ (eV)" | 0.1675 | 0.1580 | 0.1690 | 0.1683 | 0.1685 |
| electrophilicity Index "($\omega$) | 0.1318 | 0.1263 | 0.1453 | 0.1432 | 0.1433 |
| ionization potential "$I = -E_{HOMO}$ (eV)" | 0.2677 | 0.2568 | 0.2674 | 0.2672 | 0.2677 |
| electron affinity "$A = -E_{LUMO}$ (eV)" | 0.0617 | 0.0592 | 0.0707 | 0.0694 | 0.0694 |
| electronic energy "$E$ (Hartree)" | −1231.637 | −1622.651 | −804.672 | −766.595 | −1238.339 |
| chemical potential "CP" | −0.1675 | −0.14812 | −0.1691 | −0.1683 | −0.1685 |
| nucleophilicity index "N" | 7.586 | 13.50 | 6.881 | 6.984 | 6.978 |
| additional electron charge $\Delta N_{max}$ (eV) | 1.600 | 1.599 | 1.719 | 1.701 | 1.700 |

appeared at $\delta$ 167.5; however, methylene attached to ester oxygen (C-2′,2″) appeared at $\delta$ 61.0. The other carbons were also accounted for $\delta$ 29.7 (C-3′, 3″), 25.8 (C-4′,4″), 25.2 (C-5′, 5″), 38.7 (C-6′, 6″), and 27.7 (C-7′, 7″). Two terminal methyl groups appeared at $\delta$ 23.2[47] (Supporting Information, Figure S4). The mass spectrum of compound **HR5** presented a molecular peak at 390 and fragmental peaks at 27, 41, 57, 84, 104, 121, 132, 149, 167, 168, and 279. Fragment ion peaks at 279 and 167 displayed in the mass spectrum were characteristic of alkyl phthalates, and the base peak 149.0 was due to the protonated phthalic anhydride ($C_8H_5O_3$) (Supporting Information, Figure S9). Moreover, the fragmental ion pattern indicates that the under-examination molecule has formula $C_{24}H_{38}O_4$. The above NMR and GC−MS data confirm the existence and structure of compound **HR5** as bis (6-methylheptyl) phthalate (Supporting Information, Figure S10) (Mol. Weight 390).

**3.2. Biological Evaluation of Isolated Compounds.** Isolated compounds were checked for their potential as antioxidants and diabetic inhibitors by standard procedures.[30,31] Results of antidiabetic (Figure 1) revealed that the compound **HR5** was an excellent diabetic inhibitor with a minimum inhibition concentration ($IC_{50}$) of 11.69 $\mu$M, while antioxidant results (Figure 2) revealed the compounds **HR3** and **HR5** as excellent inhibitors with $IC_{50}$ = 15.14 $\mu$M and 15.64 $\mu$M, respectively, as shown in graph (Figure 2).

**3.3. QSAR Analysis.** QSAR investigation of isolated compounds (**HR1**−**HR5**) enables us to draw the fundamental upshots, which are reviewed below.

*3.3.1. Frontier Molecular Orbital Analysis.* Contour figures of highest occupied molecular orbital (HOMO) and lowest unoccupied molecular orbital (LUMO) are substantial for the prediction of molecular reactivity and pharmacological properties of compounds. HOMO and LUMO possess the tendency to donate and accept the electrons, respectively[32] (Supporting Information; Figure S11−S15), displayed the energy level and dispersion of HOMO and LUMO orbitals computed at the B3LYP/6-311G. HOMO and LUMO values anticipated that HOMO is less reactive than LUMO; however, the small energy gap revealed the softness of the molecule, which makes a molecule additionally polarized and biologically reactive in hindering the enzymatic activity. So, the small energy gap favors more chemical reactivity and less kinetic stability of a molecule.[55] LUMO and HOMO are associated with electron affinity (A) and ionization potential (I), respectively.[56]

A higher value of $E_{Homo}$ indicates the good electron-donating ability of the compound and favors better reactivity, however, a lower $E_{LUMO}$ value indicates the good electron-accepting ability of the compound and better reactivity.[32] The computed $E_{HOMO}$ values for the isolated phthalates from *H. rosa-sinensis* flowers range from −0.2677 eV for **HR1** and **HR5** to −0.2568 eV for


https://doi.org/10.1021/acsomega.3c03342
ACS Omega 2023, 8, 32677−32689

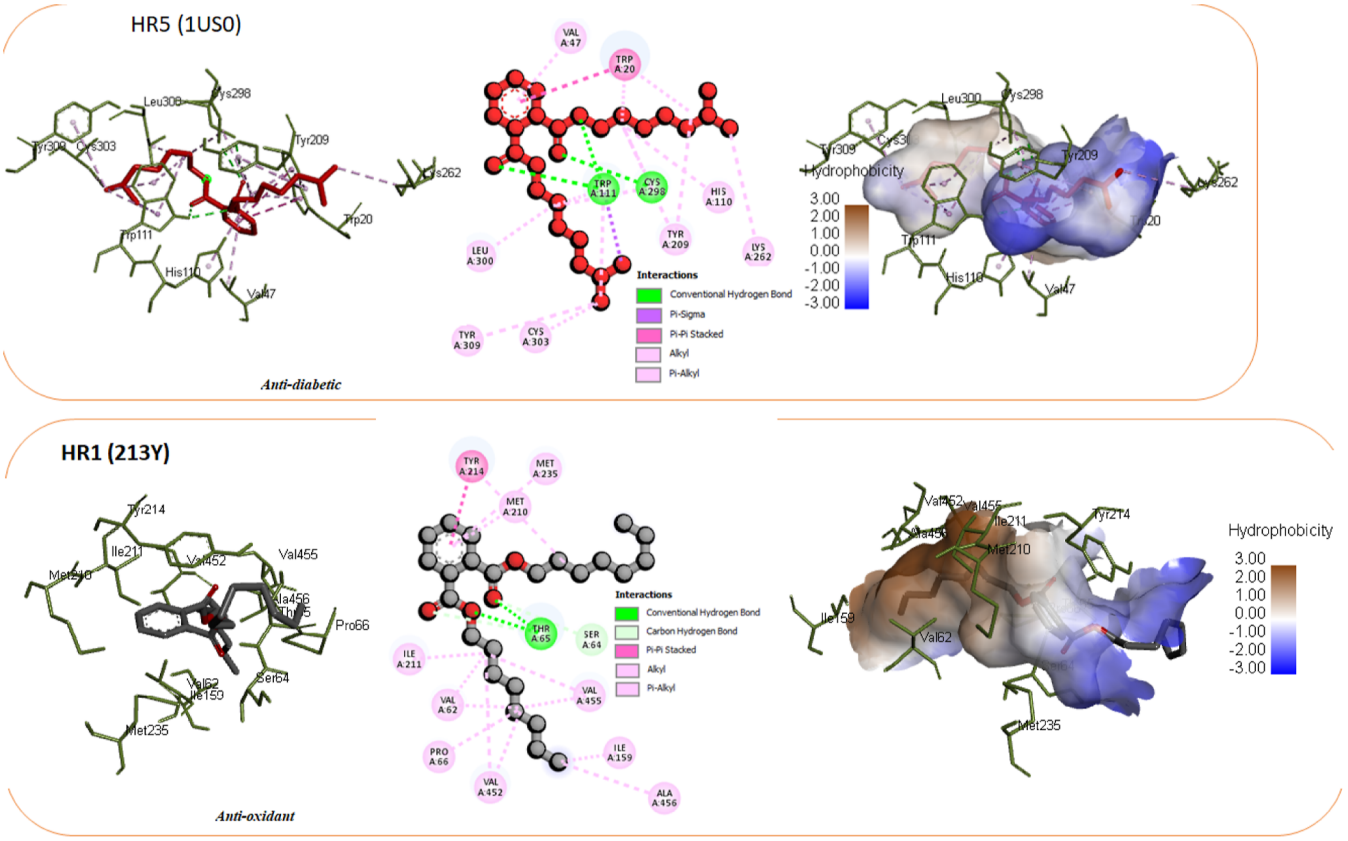


**Figure 3.** 3D visualization, 2D visualization, and hydrophobic interactions of the binding framework of protein−ligand interactions of **HR5** for enzyme aldose reductase (PDB ID: 1US0); 3D visualization, 2D visualization, and hydrophobic interactions of the binding framework of protein−ligand interactions of **HR1** for glutathione peroxidase (PDB ID: 2I3Y) The antioxidant potential of phthalates was evaluated by docking against glutathione peroxidase and superoxide dismutase cocrystal structures downloaded from the PDB database.

**HR2.** Thus, the activity status of under-studied compounds with the increase in $E_{Homo}$ value is as follows:

Compound **HR2** > Compound **HR4** > Compound **HR3** > Compound **HR1** = Compound **HR5**

The computed $E_{LUMO}$ values for the isolated phthalates range from −0.0707 eV for **HR3** to −0.0592 eV for **HR2** (Supporting Information, Figures S11−S15). Thus, the activity status of under-studied compounds with the increase in $E_{LUMO}$ value is as follows:

Compound **HR3** > Compound **HR4** = Compound **HR5** > Compound **HR1** > Compound **HR2**

Rendering Table 2, the parameter in third place is the energy gap ($\Delta E$) between $E_{Homo}$ and $E_{LUMO}$. The compound **HR3** possesses the lowest energy gap ($\Delta E_{gap}$ = 0.19721 eV) among all five under discussion compounds which makes compound **HR3** softer ($S$ = 5.084 eV), least hard ($\eta$ = 0.0983 eV), and more reactive as compared to other isolated compounds.[55]

*3.3.2. Global Reactivity Descriptors.* The calculated values of reactivity parameters like electronegativity ($\chi$), dipole moment ($\mu$), electrophilicity index ($\omega$), electronic energy (E), chemical Potential (CP), ionization potential (I), electronic charges ($\Delta N_{max}$), and nucleophilicity index (N) for each isolated phthalate are shown in Table 2. ΔNmax represents the charge of molecules. A compound with a higher value of $\Delta N_{max}$ is considered more active biologically. Charge density and bond properties of compounds can be described by the dipole moment ($\mu$). Figure S16 displays the vector of the dipole moment ($\mu$) of all isolated compounds. Among the isolated phthalate compounds, **HR3** has the highest dipole moment ($\mu$ = 3.682993) which depicts that this compound owns excellent distribution of charge and increasing bond distance as compared to the other four under-studied compounds. It means that compound **HR3** displayed excellent conductivity enhanced by oxidation.[57−60] The highest electronegativity ($\chi$) and electrophilicity ($\omega$) values (0.1690 and 0.1453 eV) suggest that compound **HR3** is the paramount electrophile or has the best ability to accept electrons.[61] The compound **HR3** is the most stable phthalate as compared to other under discussion compounds as it possesses the highest value of electronic energy (E) which suggested that dipole−dipole interactions, Coulombic forces, and hydrogen bonds contributed toward the more solute−solvent interaction, greater binding affinity, and less $IC_{50}$ value.[58]

*3.3.3. Molecular Electrostatic Potential.* MEP aids in prophesying the molecular recognition procedure, hydrogen bonding interaction, and explanation of nucleophilic and electrophilic reactions. It also helps to recognize various types of biological interactions such as drug−protein interactions and molecular docking, etc. Figure S17 (Supporting Information) represents the MEP of extracted phthalates **HR1**, **HR2**, **HR3**, **HR4**, and **HR5** based on SCF energy. In a biological setup, MEP displays the behavior and response of molecules toward the active binding sites. MEP is a visual pattern to predict the polarity of a compound. The negative (yellow and red) and positive (blue) sections of MEP exhibited the sites of electrophilic and nucleophilic reactivity, respectively.[62] So, it is clear from MEP structures of all isolated compounds that there is a positive or blue region around all


https://doi.org/10.1021/acsomega.3c03342
ACS Omega 2023, 8, 32677−32689

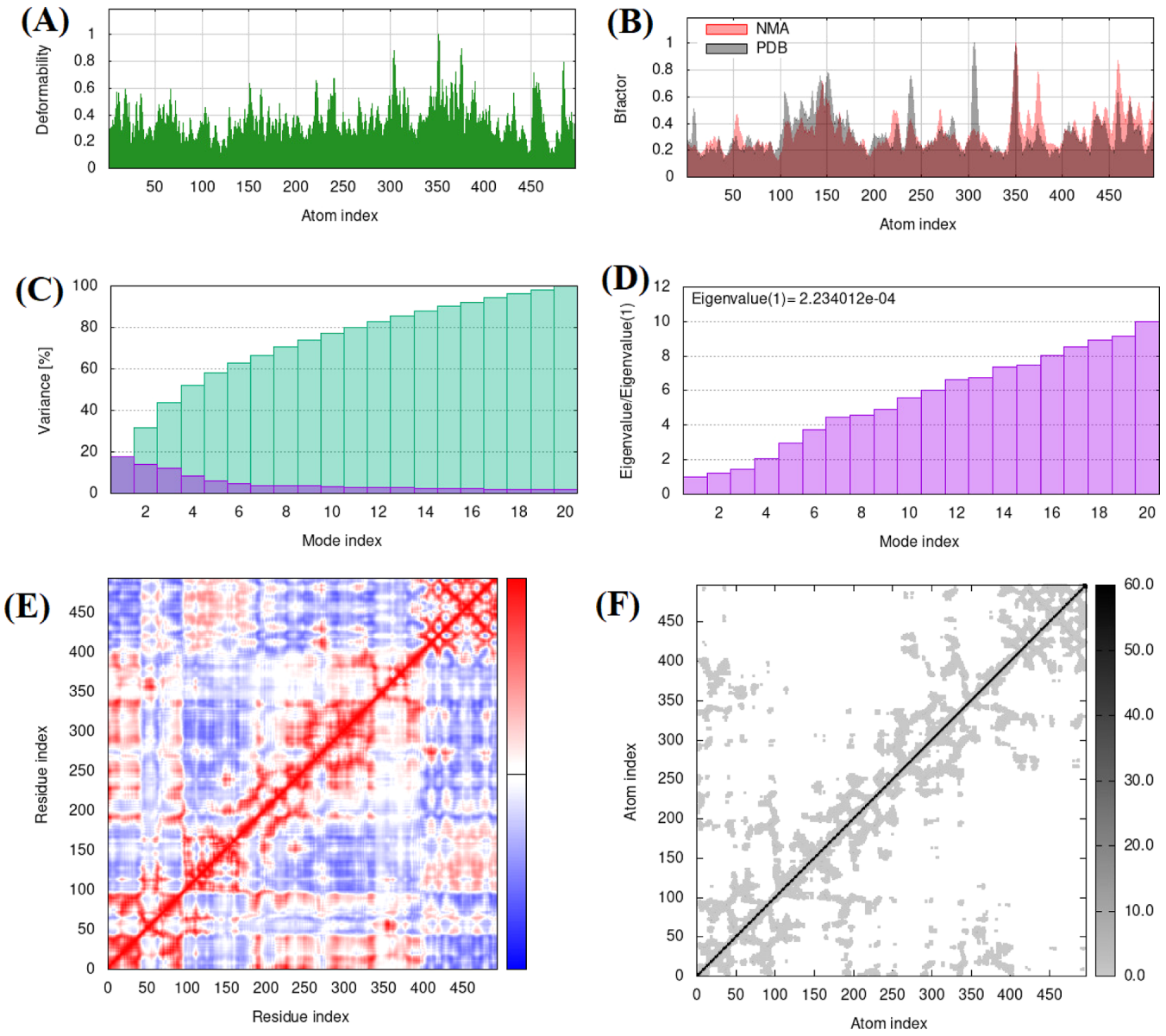


**Figure 4.** Upshots of molecular dynamics simulation of glucokinase (1HNY)−HR5 docked complex (A) Deformability, (B) *B*-factor, (C) variance, (D) eigenvalues, (E) co-variance plot, and (F) elastic network model.

hydrogen atoms as hydrogen possesses the tendency to react with a nucleophile; however, there is a negative or red region around the oxygen atom due to the capability of oxygen to react with an electrophile. The green color of benzene rings in MEP is an indication of its neutral reactivity.[63]

**3.4. Molecular Docking Simulation.** The biological potential of compounds by utilization of conceivable conformations and orientations for the binding sites of ligands can be assessed by performing molecular docking. The molecular docking of isolated phthalates **HR1−HR5** was investigated by utilizing Auto Dock Vina.[64] In order to explore the biological potential of isolated compounds, first, standard compounds (metformin and quercetin as reference for antidiabetic and antioxidant potential, respectively) of corresponding protein were docked to standardize the protocol.[65] Antidiabetic potential of phthalates was evaluated for performing the inhibitory action of human pancreatic $\alpha$-amylase by docking phthalates into the active site of receptor proteins. The binding affinity score of all compounds was more than that of standard metformin. All the compounds showed van der Waals interactions in the form of pi−pi, alkyl, pi−sigma, pi−sulfur, and pi−cation which were electrostatic and hydrophobic in nature.[64] The docking protocol provided variable binding affinity values for each compound, as shown in the table. Table S2, Supporting Information, showed that the lowest binding affinity was shown by **HR2 and HR4** ($\Delta G$ = −5.2 kcal/mol). **HR3** showed slightly greater binding affinity for receptor protein 1HNY than **HR2 and HR4** ($\Delta G$ = −5.3 kcal/mol). **HR1** also show slightly large $\Delta G$ = −5.8 kcal/mol, while **HR5** showed $\Delta G$ = −5.9 kcal/mol, due to charge neutrality and more alkyl and pi interactions.[66] So, of all the compounds **HR5** showed the best binding affinity with 1HNY (Supporting Information, Figures S14 and S15), it was concluded that **HR5** can be a lead compound for inhibiting the human pancreatic $\alpha$-amylase activity.[67]

Table S2 (Supporting Information) showed the conventional and van der Waals interactions of docked phthalates with the cocrystal structure of glutathione peroxidase (PDB



https://doi.org/10.1021/acsomega.3c03342
ACS Omega 2023, 8, 32677−32689

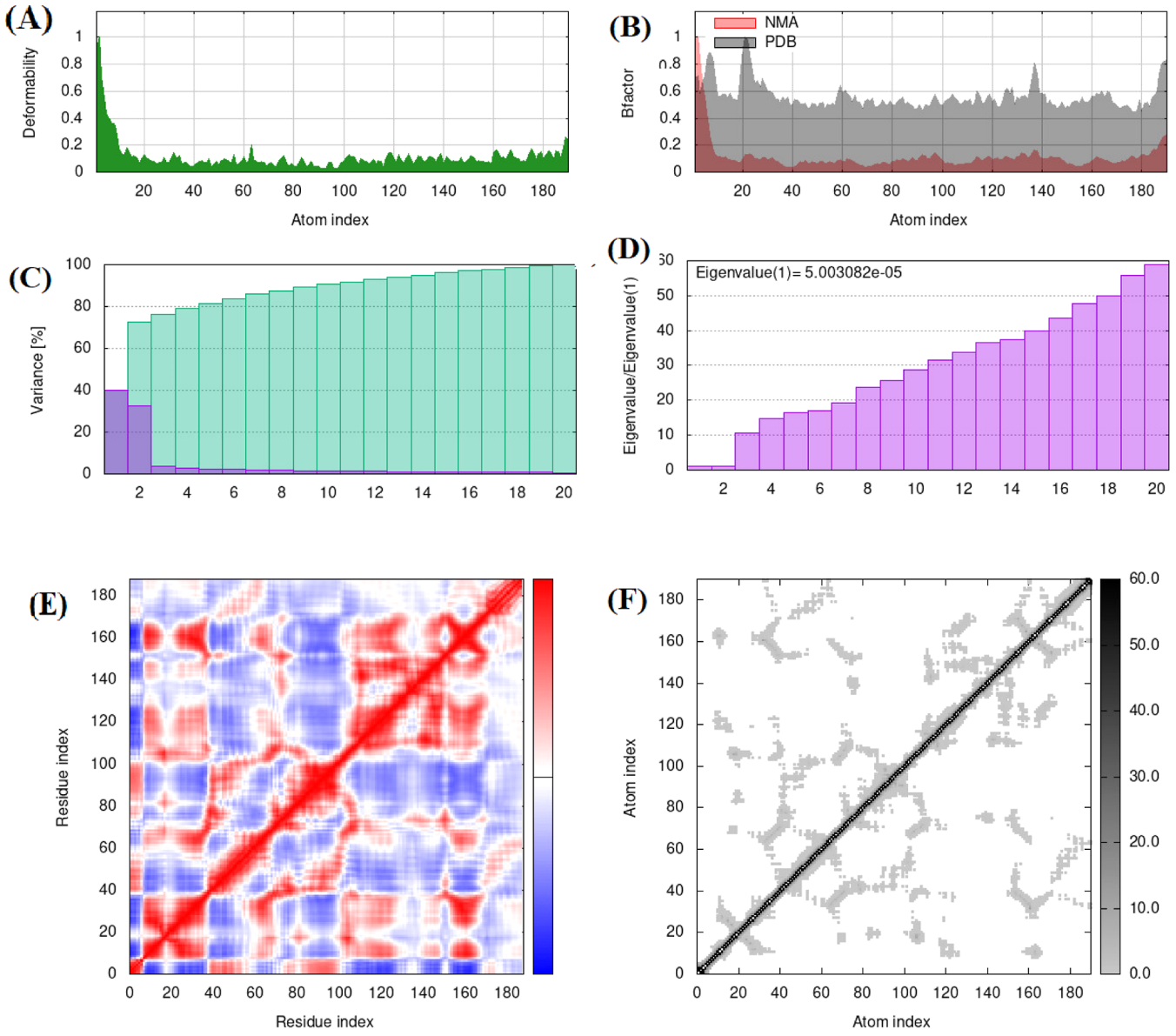


**Figure 5.** Upshots of molecular dynamics simulation of glutathione peroxidase (2I3Y)−HR1 docked complex (A) deformability, (B) *B*-factor, (C) variance, (D) eigenvalues, (E) co-variance plot, and (F) elastic network model.

ID: 2I3Y). Compound **HR1** was the best docked and scored compound for inhibiting the glutathione peroxidase by forming four hydrogen bonds with His200 and Arg201, located in a hydrophobic pocket of glutathione peroxidase surrounded by residues HIS200, ILE162, TRP181, and ARG180 (Figure 3).[66,68] While remaining compounds also showed nearly the same $\Delta G$ values, i.e., −4.3−5.3 kcal/mol (Supporting Information, Figures S20 and S21). The binding affinity score $\Delta G$ for phthalates ranged from −4.1 to −5.0 kcal/mol. Compound **HR2** possessed the lowest binding affinity score of −5.1 kcal/mol, thus indicating the highest potential for inhibiting the superoxide dismutase, shown in the Table S2 (Supporting Information). While the other four phthalates have comparable binding affinity scores $\Delta G$ for inhibiting the enzymatic activity of 5O40, having conventional, electrostatic, and hydrophobic interactions.[68,69]

**3.5. Molecular Dynamic Simulations.** Figures 4−6 represent the results of molecular dynamics simulation. NMA (normal-mode analysis) was utilized by the IMOD server to analyze the stability of top-ranked docked protein-ligand complexes on the base on inner coordinates. The stability of complexes was displayed by plots describing various parameters like deformability, *B*-factors, eigenvalues, covariance plot, and elastic network templates.

*3.5.1. 1HNY−HR5 Complex.* The main chain deformability plot, generated as a result of MD simulation of the 1HNY−**HR5** docked complex (Figure 4A), displays fluctuations for all residues, representing high deformability. The pointy area of peaks termed as hinges are locations of interaction of protein 1HNY and **HR5**. The *B*-factor plots displays peaks for the *B*-factor as well as for the NMA simulations. The *B*-factor measures protein flexibility and computes the uncertainty of each atom. The *B*-factor plots are the visual representation of interaction of the complex among the PDB and NMA sector.[70] The plot shows almost the similar peak pattern, which is the indication of similarity in the simulation and the experimental upshots from PDB (Figure 4B). The plot of variance displays the higher level of individual variance (approximately 19%),


https://doi.org/10.1021/acsomega.3c03342
ACS Omega 2023, 8, 32677−32689

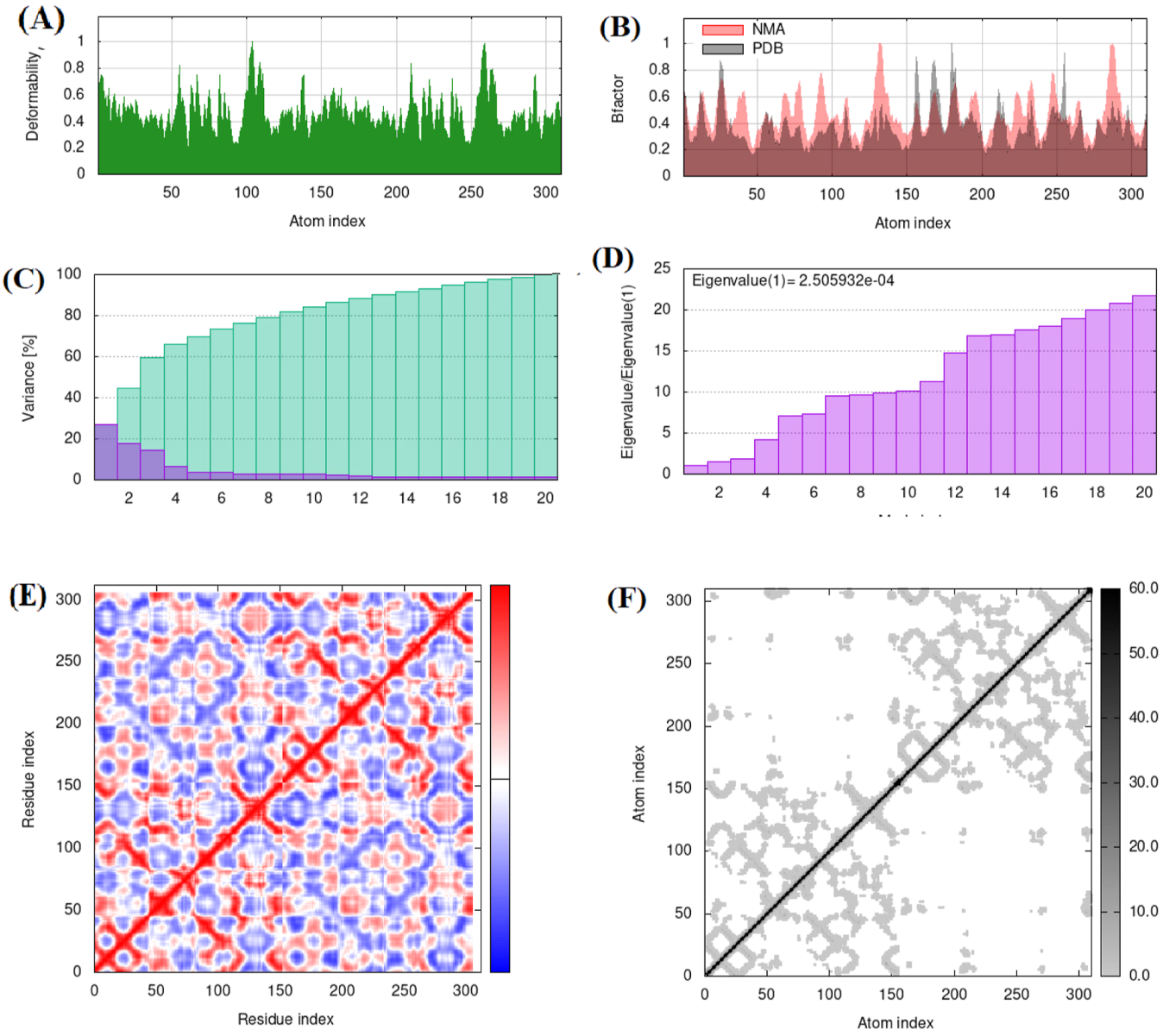


**Figure 6.** Upshots of molecular dynamics simulation of superoxide dismutase (5O40)−HR2 docked complex (A) deformability, (B) *B*-factor, (C) variance, (D) eigenvalues, and (E) co-variance plot. (F) elastic network model.

which indicates the lower eigenvalue as variance and eigenvalue have inverse relation to each normal mode (Figure 4C).[71] The eigenvalue displays the amount of energy needed to distort a structure, so it is intuitive of the mobility stiffness of the residues of protein. The obtained eigenvalue for the complex 1HNY-**HR5** was $2.23 \times 10^{-4}$, which can be considered very low (Figure 4D). This very low eigenvalue proves the strong interaction between 1HNY and **HR5** and results in the formation of a stable complex. Next, the covariance plot exhibits noncorrelation, correlation and anticorrelation motion by utilizing white, red, and blue color codes, respectively.[72] The covariance plot displays that the underdiscussion complex had a mixture of more high and low interacting residues in contrast to noninteractive ones as it exhibits blatant dark red and light blue colors (Figure 4E). The elastic network plot describes the rigidness of the target 1HNY. As light gray color can be noticed in elastic network plot, the stiffness of this protein is low and it can be deformed easily (Figure 4F).

*3.5.2. Glutathione Peroxidase 2I3Y-**HR1** Complex.* The main chain deformability plot generated as a result of MD simulation of 2I3Y−**HR1** docked complex displays minor fluctuations, representing low deformability (Figure 5A). The pointy areas called hinges are the locations of interaction of 2I3Y and **HR1** with one another. The *B*-factor plot displays that the obtained peak patterns are nearly similar (Figure 5B). The variance plot (Figure 5C) displays the higher level of individual variance (approximately 40%). The obtained eigenvalue for complex 2I3Y−**HR1** was the highest among all complexes, $5.0 \times 10^{-5}$, which is considered lower (Figure 5D). It is an indication that the interaction between 2I3Y and **HR1** is excellent. Thus, complex 2I3Y−**HR1** is considered comparatively less stable. The covariance plot displays prominent blue and red color, so it can be deduced that 2I3Y−**HR1** complex had higher number of interacting and noninteracting residues (Figure 5E). The elastic network plot describes the rigidness of the target 2I3Y. As a light gray color



https://doi.org/10.1021/acsomega.3c03342
*ACS Omega* 2023, 8, 32677−32689

can be noticed in the elastic network plot, the stiffness of this protein is low and it can be deformed easily (Figure 5F).

*3.5.3. Superoxide Dismutase (5O40)−**HR2** Complex.* The main chain deformability plot generated as a result of MD simulation of the 5O40−**HR2** docked complex displays fluctuations for all residues, representing high deformability (Figure 6A). The pointy areas of peaks termed as hinges are the locations of interaction of protein 5O40 and **HR2**. The *B*-factor plot shows almost a similar peak pattern (Figure 6B). The plot of variance displays the higher level of individual variance (approximately 26%), which directs the lower eigenvalue (Figure 6C). The obtained eigenvalue for the complex 5O40−**HR2** was $2.5 \times 10^{-4}$, which directs better flexibility and stability of complex. The covariance plot displays prominent blue and red color, so it can be deduced that 5O40−**HR2** complex had higher number of interacting and noninteracting residues (Figure 6E). The elastic network plot describes the rigidness of target 5O40. The visibility light gray color in elastic network plot, confirms that this protein has low stiffness, and it can be deformed easily (Figure 6F).

## 4. CONCLUSIONS

Phthalates have been used as plasticizers for decades and are obtained synthetically as well as naturally. Most of the research represents their polymer use only. There has been no work on its biological importance for use in the pharmaceutical industry. With the research evolution, phthalates are becoming environmental pollutants as plasticizers; there is a need to use them in another way to repurpose their use. To repurpose them, the present study checked them for their potential to use in the pharmaceutical industry. Their evaluation as antidiabetic and antioxidant agents showed that these could be used as drugs because their activity meets that of standard drugs. Among all fractions, two fractions were subjected to column chromatography and five compounds were purified. The structure elucidation of these compounds confirmed their structures as phthalates (**HR1**−**HR5**) by $^{1}$H NMR, $^{13}$C NMR, and GC−MS spectral data. **HR5** showed excellent inhibition against diabetes, while **HR1** showed fair inhibition and **HR2**−**HR4** showed moderate antidiabetic results. In comparison, oxidant inhibition results showed that **HR1** and **HR2** were explored as excellent inhibitors of glutathione peroxidase and superoxide dismutase, respectively. Collectively, as almost all of the ligands exhibited good antidiabetic and antioxidant potential (in in vitro and in silico experiments) against all selected protein targets, they can be claimed as broad-spectrum antidiabetic and antioxidant agents. Future work will be on their metabolism to make them effective drugs.

## ■ ASSOCIATED CONTENT

### Supporting Information

The Supporting Information is available free of charge at https://pubs.acs.org/doi/10.1021/acsomega.3c03342.

Preparation of crude extract of flowers; schematic representation of column chromatography of the ethyl acetate extract; column chromatography of fraction PSHR III; column chromatography of fraction RSHR I;$^{1}$H NMR and $^{13}$C NMR spectra; GC−MS spectra; structures of isolated compounds; contour diagrams of FMOs; optimized geometry of structures; MEP of the compounds; 3D visualization, 2D visualization, and hydrophobic interactions of the binding framework; instrumental specifications and analysis conditions for GC−MS analysis; and depicted molecular interactions of rigid protein ligand docking of phthalates with their chemical structures (PDF)

## ■ AUTHOR INFORMATION


### Corresponding Authors

**Nusrat Shafiq** − *Synthetic and Natural Products Discovery (SNPD) Laboratory, Department of Chemistry, Government College Women University, Faisalabad 38000, Pakistan*; Email: dr.nusratshafiq@gcwuf.edu.pk

**Mohammed Bourhia** − *Department of Chemistry and Biochemistry, Faculty of Medicine and Pharmacy, Ibn Zohr University, Laayoune 70000, Morocco*; orcid.org/0000-0003-3707-8461; Email: bourhiamohammed@gmail.com

### Authors

**Farah Yasmin** − *Synthetic and Natural Products Discovery (SNPD) Laboratory, Department of Chemistry, Government College Women University, Faisalabad 38000, Pakistan*

**Zill-i-Huma Nazli** − *Department of Chemistry, Government College Women University, Faisalabad 38000, Pakistan*

**Maryam Aslam** − *Green Chemistry Laboratory, Department of Chemistry, Government College Women University, Faisalabad 38000, Pakistan*

**Yousef A. Bin Jardan** − *Department of Pharmaceutics, College of Pharmacy, King Saud University, Riyadh 11451, Saudi Arabia*

**Hiba-Allah Nafidi** − *Department of Food Science, Faculty of Agricultural and Food Sciences, Laval University, Quebec City G1 V 0A6 Quebec, Canada*

Complete contact information is available at: https://pubs.acs.org/10.1021/acsomega.3c03342


### Author Contributions

F.Y. = drafting of manuscript and performing experiments; Z.-i.-H.N. = supervision and proofreading; N.S. = conceptualization of idea, write up, and finalizing the article; M.A. = proof reading. Y.A.B.J., H.-A.N., and M.B.: writing the original draft, formal analysis, investigations, funding acquisition, and resource.


### Funding

Authors are thankful to Higher Education Commission of Pakistan to provide facilities to conduct this research under HEC/TDF03−172 research Grant. This work was financially supported by the Researchers Supporting Project (RSP2023R457). King Saud University, Riyadh, Saudi Arabia


### Notes

The authors declare no competing financial interest.
Samples are available.

## ■ ACKNOWLEDGMENTS


The authors would like to extend their sincere appreciation to the Researchers Supporting Project, King Saud University, Riyadh, Saudi Arabia for funding this work through the project number (RSP2023R457). Authors are thankful to Government College University Lahore for providing the facility of GC−MS, Quaid-e-Azam University Islamabad for the NMR facility, and the Higher Education Commission of Pakistan for providing facilities to conduct this research under HEC/TDF03-172 Research Grant.

## REFERENCES


(1) Allahresani, A.; Ghorbanian, F.; Kazemnejadi, M.; Nasseri, M. A. Phytochemical studies of Cynodon dactylon (L.) and isolation and characterization of bis (2-ethylheptyl) phthalate from the plant. *Asian J. Green Chem.* **2021**, *5* (1), 23−38.

(2) Romeh, A. A. Diethyl phthalate and dioctyl phthalate in Plantago major L. *Afr. J. Agric. Res.* **2013**, *8* (32), 4360−4364.

(3) Saeidnia, S.; Abdollahi, M. *Are Medicinal Plants Polluted With Phthalates?*; Springer, 2013.

(4) Roy, R. N. Bioactive natural derivatives of phthalate ester. *Crit. Rev. Biotechnol.* **2020**, *40* (7), 913−929.

(5) Shafiq, N.; Yasmin, F.; Noreen, S.; Shahzad, A.; Nazli, Z. I. h.; Parveen, S.; Ali, B.; Ahmad, Z.; Rashid, M.; Bilal, M. Phytochemical Profiling of Medicinal Plants Extracts and Their Antioxidant and Anticancer Potentialities Against Human Liver Cancer (Hep G2) Cell Lines. *Rev. Chim.* **2021**, *72* (1), 100−110.

(6) Joshi, A.; Bhobe, M.; Sattarkar, A. Phytochemical investigation of the roots of Grewia microcosLinn. *J. Chem. Pharm. Res.* **2013**, *5* (7), 80−87.

(7) Ortiz, A.; Sansinenea, E. Di-2-ethylhexylphthalate may be a natural product, rather than a pollutant. *J. Chem.* **2018**, *2018*, 1−7.

(8) Visht, S.; Chaturvedi, S. Isolation of natural products. *J. Curr. Pharma Res.* **2012**, *2* (3), 584−599.

(9) Vuorela, P.; Leinonen, M.; Saikku, P.; Tammela, P.; Rauha, J.-P.; Wennberg, T.; Vuorela, H. Natural products in the process of finding new drug candidates. *Curr. Med. Chem.* **2004**, *11* (11), 1375−1389.

(10) Koparde, A. A.; Doijad, R. C.; Magdum, C. S. Natural products in drug discovery. *Pharmacognosy-Medicinal Plants*; IntechOpen, 2019.

(11) Konappa, N.; Udayashankar, A. C.; Krishnamurthy, S.; Pradeep, C. K.; Chowdappa, S.; Jogaiah, S. GC-MS analysis of phytoconstituents from Amomum nilgiricum and molecular docking interactions of bioactive serverogenin acetate with target proteins. *Sci. Rep.* **2020**, *10* (1), 16438−16523.

(12) Missoum, A. An update review on Hibiscus rosa sinensis phytochemistry and medicinal uses. *J. Ayurvedic Herb. Med.* **2018**, *4* (3), 135−146.

(13) Khadiga G Abd Elaleem, E. A. S.; Abd Elaleem, H. G.; Abd Elaleem, H. G. Potential Antibacterial Activity of Hibiscus rosa sinensis Linn flowers extracts. *Int. J. Curr. Microbiol. Appl. Sci.* **2017**, *6* (4), 1066−1072.

(14) Khalid, L.; Rizwani, G. H.; Sultana, V.; Zahid, H.; Khursheed, R.; Shareef, H. Antidepressant activity of ethanolic extract of Hibiscus rosa sinenesis Linn. *Pak. J. Pharm. Sci.* **2014**, *27* (5), 1327−1331.

(15) Gupta, V.; Bansal, P.; Garg, A.; Meena, A. Pharmacopoeial standardization of Hibiscus rosa sinensis Linn. *Int. J. Pharm. Clin. Res.* **2009**, *1* (3), 124−126.

(16) Jasiem, T. M.; Nasser, N. M.; Baderden, S. K.; Hasan, H. A. In Pharmacognostical and phytochemical studies of Iraqi Hibiscus rosa-sinensis; *AIP Conference Proceedings*, AIP Publishing LLC: 2019; p 040002.

(17) Patel, S.; Adhav, M. Comparative phytochemical screening of ethanolic extracts (flower and leaf) of morphotypes of Hibiscus Rosa-sinensis Linn. *J. Pharmacogn. Phytochem.* **2016**, *5* (3), 93−95.

(18) Arullappan, S.; Zakaria, Z.; Basri, D. F. Preliminary screening of antibacterial activity using crude extracts of Hibiscus rosa sinensis. *Trop. Life Sci. Res.* **2009**, *20* (2), 109−118.

(19) Begum, Z.; Younus, I.; Ali, S. Anti-inflammatory, analgesic and anti-pyretic activities of Hibiscus rosa-sinesnsis Linn and phytochemicals. *World J. Pharm. Pharm. Sci.* **2015**, *4* (12), 116−123.

(20) Falade, O. S.; Aderogba, M. A.; Kehinde, O.; Akinpelu, B. A.; Oyedapo, B.; Adewusi, S. Studies on the chemical constituents, antioxidants and membrane stability activities of Hibiscus rosa sinensis. *Niger. J. Nat. Prod. Med.* **2009**, *13* (1), 58−64.

(21) Agarwal, S.; Prakash, R. Evaluation of Antibacterial activity of Hibiscus rosa-sinensis flower extract against E. coli and B. subtillis. In *Biological Forum*; Citeseer, 2014, p 194.

(22) Upadhyay, S.; Upadhyay, P. Hibiscus rosa-sinensis: pharmacological review. *Int. J. Res. Pharm. Biomed. Sci.* **2011**, *2* (4), 1449−1450.

(23) Shafiq, N. *Chemical and Biological Screening of Seriphidium stenocephalum Steriphidium Oliverianum and Rumex Hastattus*; Islamia University: Bahawalpur, 2014.

(24) Sharma, N.; Sharma, A.; Bhatia, G.; Landi, M.; Brestic, M.; Singh, B.; Singh, J.; Kaur, S.; Bhardwaj, R. Isolation of phytochemicals from Bauhinia variegata l. Bark and their in vitro antioxidant and cytotoxic potential. *Antioxidants* **2019**, *8* (10), 492.

(25) Khayruzamri, M. A.; Samsudin, W. N. A. W. M.; Hashim, S. E. Phytochemicals and Antioxidant Activity of Anacardium Occidentale. *J. Sci. Math. Lett.* **2023**, *11*(1), 59-63.

(26) Arullappan, S.; Sawai, S.; Chee, A.; Mahandan, M.; Shanmugavelan, R. Phytochemical Screening and Evaluation of Cytotoxic Effect and Antioxidant Activity of Fractions Isolated from Stenochlaena palustri (Burm.f.) Bedd. Leaves. *Indian J. Pharm. Educ. Res.* **2017**, *51*, 735−740.

(27) Graça, V.; Calhelha, R. C.; Nunes, F. M.; Berthet, J.; Ferreira, I. C.; Santos, P. Isolation of secondary metabolites from Geranium molle L. with anticancer potential. *Ind. Crops Prod.* **2019**, *142* (111859), 111859.

(28) Hussain, F.; Shahid, M.; Javed, K. Antioxidant, antiglycation and alpha Amylase inhibitory activities of Cassia absus seeds. *Int. Sci. Org. Curr. Sci. Perspect.* **2015**, *2* (1), 5−9.

(29) Sudha, P.; Zinjarde, S. S.; Bhargava, S. Y.; Kumar, A. R. Potent $\alpha$-amylase inhibitory activity of Indian Ayurvedic medicinal plants. *BMC Complementary Altern. Med.* **2011**, *11* (1), 5.

(30) Arshad, U.; Ahmed, S.; Shafiq, N.; Ahmad, Z.; Hassan, A.; Akhtar, N.; Parveen, S.; Mehmood, T. Structure-Based Designing, Solvent Less Synthesis of 1, 2, 3, 4-Tetrahydropyrimidine-5-carboxylate Derivatives: A Combined In Vitro and In Silico Screening Approach. *Molecules* **2021**, *26* (15), 4424.

(31) Zarren, G.; Shafiq, N.; Arshad, U.; Rafiq, N.; Parveen, S.; Ahmad, Z. Copper-catalyzed one-pot relay synthesis of anthraquinone based pyrimidine derivative as a probe for antioxidant and antidiabetic activity. *J. Mol. Struct.* **2021**, *1227*, 129668.

(32) Kolawole, O. A.; Benjamin, A. B. Theoretical Investigation on Biological Activity of Phenacetin and Its Derivatives via DFT and Docking Approach. *J. Chem. Pharm. Res.* **2019**, *25* (3), 1−7.

(33) Srivastava, A. K.; Misra, N. A comparative theoretical study on the biological activity, chemical reactivity, and coordination ability of dichloro-substituted (1, 3-thiazol-2-yl) acetamides. *Can. J. Chem.* **2014**, *92* (3), 234−239.

(34) Deller, M. C.; Rupp, B. Models of protein-ligand crystal structures: trust, but verify. *J. Comput.-Aided Mol. Des.* **2015**, *29*, 817−836.

(35) Angadi, K. K.; Gundampati, R. K.; Jagannadham, M. V.; Kandru, A. Molecular docking studies of guggultetrol from Nymphaea pubescens with target glucokinase (GK) related to type-II Diabetes. *J. Appl. Pharm. Sci.* **2013**, *3* (2), 127−131.

(36) Aanouz, I.; Belhassan, A.; El-Khatabi, K.; Lakhlifi, T.; El-Ldrissi, M.; Bouachrine, M. Moroccan Medicinal plants as inhibitors against SARS-CoV-2 main protease: Computational investigations. *J. Biomol. Struct. Dyn.* **2021**, *39* (8), 2971−2979.

(37) Khayrani, A. C.; Irdiani, R.; Aditama, R.; Pratami, D. K.; Lischer, K.; Ansari, M. J.; Chinnathambi, A.; Alharbi, S. A.; Almoallim, H. S.; Sahlan, M. Evaluating the potency of Sulawesi propolis compounds as ACE-2 inhibitors through molecular docking for COVID-19 drug discovery preliminary study. *J. King Saud Univ., Sci.* **2021**, *33* (2), 101297.

(38) Schultz, P. G.; Wang, L. *The Scripps Research Institute (La Jolla, CA)*; The Scripps Research Inst.: La Jolla, CA (United States), 2010.

(39) Joshi, T.; Joshi, T.; Sharma, P.; Chandra, S.; Pande, V. Molecular docking and molecular dynamics simulation approach to screen natural compounds for inhibition of Xanthomonas oryzae pv. Oryzae by targeting peptide deformylase. *J. Biomol. Struct. Dyn.* **2021**, *39* (3), 823−840.

(40) Afriza, D.; Suriyah, W.; Ichwan, S. In silico analysis of molecular interactions between the anti-apoptotic protein survivin and dentatin, nordentatin, and quercetin; *Journal of Physics: Conference Series*, IOP Publishing, 2018; p 032001.




https://doi.org/10.1021/acsomega.3c03342
*ACS Omega* 2023, 8, 32677−32689

(41) Zulqurnain, M.; Fahmi, M. R. G.; Fadlan, A.; Santoso, M. Synthesis and Molecular Docking Study of Pyrazine-2-carboxylic acid Derivatives;. In *IOP Conference Series: Materials Science and Engineering*; IOP Publishing, 2020; p 012057.
(42) Parveen, S.; Alnoman, R. B.; Bayazeed, A. A.; Alqahtani, A. M. Computational Insights into the Drug Repurposing and Synergism of FDA-approved Influenza Drugs Binding with SARS-CoV-2 Protease against COVID-19. *Am. J. Microbiol. Res* **2020**, *8* (3), 93−102.
(43) Pokharkar, O.; Lakshmanan, H.; Zyryanov, G.; Tsurkan, M. In silico evaluation of antifungal compounds from marine sponges against COVID-19-associated mucormycosis. *Mar. Drugs* **2022**, *20* (3), 215.
(44) Santra, D.; Maiti, S. Molecular dynamic simulation suggests stronger in-silico docking of Omicron spike on ACE2 than Wild but weaker than Delta SARS-CoV-2 variants can be blocked by engineered S1-RBD fraction. *Struct. Chem.* **2022**, *33* (5), 1755−1769.
(45) Dashputre, N. L.; Kakad, S. P.; Chaudhari, P. B. Molecular Modeling Studies Approach Against Enzymes Causing Alzheimer's Disease Using Hancorniaspeciosa Linn By Molecular Docking And Molecular Dynamics Simulations Techniques. *J. Pharm. Negat. Results* **2022**, *13* (5), 2233−2240.
(46) Rajiniraja, M.; Sivaramakrishna, A.; Sabareesh, V.; Jayaraman, G. In vitro inhibition potential of mono-n-octyl phthalate on Mycobacterium tuberculosis H37Ra: Possibility of binding to mycobacterial PknB—An in silico approach. *Biotechnol. Appl. Biochem.* **2018**, *65* (6), 865−875.
(47) Rajkumar, T.; Manimaran, M.; Taju, G.; Vimal, S.; Majeed, S. A.; Kannabiran, K.; Sivakumar, S.; Kumar, K.; Madhan, S.; Hameed, A. S. Antiviral viral compound from Streptomyces ghanaensis like strain against white spot syndrome virus (WSSV) of shrimp. *BioRxiv* **2018**, *2018*, 340265.
(48) Pladio, L. P.; Villaseñor, I. Anti-spasmodic constituents from drimys piperita hook F. Leaves. *Philipp. J. Sci.* **2004**, *133* (1), 17−21.
(49) Russo, M. V.; Avino, P.; Perugini, L.; Notardonato, I. Extraction and GC-MS analysis of phthalate esters in food matrices: a review. *RSC Adv.* **2015**, *5* (46), 37023−37043.
(50) Malarvizhi, D.; Anusooriya, P.; Meenakshi, P.; Sundaram, S.; Oirere, E.; Gopalakrishnan, V. K. Isolation, structural characterization of oleic acid from Zaleya decandra root extract. *Anal. Chem. Lett.* **2016**, *6* (5), 669−677.
(51) Monakhova, Y. B.; Kuballa, T.; Leitz, J.; Lachenmeier, D. W. Determination of diethyl phthalate and polyhexamethylene guanidine in surrogate alcohol from Russia. *Int. J. Anal. Chem.* **2011**, *2011*, 1−7.
(52) Mangamuri, U.; Muvva, V.; Poda, S.; Naragani, K.; Munaganti, R. K.; Chitturi, B.; Yenamandra, V. Bioactive metabolites produced by Streptomyces Cheonanensis VUK-A from Coringa mangrove sediments: isolation, structure elucidation and bioactivity. *3 Biotech* **2016**, *6* (1), 63−68.
(53) Shen, H. Y.; Jiang, H. L.; Mao, H. L.; Pan, G.; Zhou, L.; Cao, Y. F. Simultaneous determination of seven phthalates and four parabens in cosmetic products using HPLC-DAD and GC-MS methods. *J. Sep. Sci.* **2007**, *30* (1), 48−54.
(54) Jaworek, K.; Czaplicka, M. Determination of phthalates in polymer materials-comparison of GC/MS and GC/ECD methods. *Polimeros* **2013**, *23* (6), 718−724.
(55) Bendjeddou, A.; Abbaz, T.; Gouasmia, A.; Villemin, D. Molecular structure, HOMO-LUMO, MEP and Fukui function analysis of some TTF-donor substituted molecules using DFT (B3LYP) calculations. *Int. Res. J. Pure Appl. Chem.* **2016**, *12*, 1−9.
(56) O Ozdemir, U.; Ilbiz, F.; Balaban Gunduzalp, A.; Ozbek, N.; Karagoz Genç, Z.; Hamurcu, F.; Tekin, S. Alkyl sulfonic acide hydrazides: Synthesis, characterization, computational studies and anticancer, antibacterial, anticarbonic anhydrase II (hCA II) activities. *J. Mol. Struct.* **2015**, *1100*, 464−474.
(57) Sayin, K.; Üngördü, A. Investigation of anticancer properties of caffeinated complexes via computational chemistry methods. *Spectrochim. Acta, Part A* **2018**, *193*, 147−155.
(58) Honarparvar, B.; Pawar, S. A.; Alves, C. N.; Lameira, J.; Maguire, G. E.; Silva, J. R. A.; Govender, T.; Kruger, H. G. Pentacycloundecane lactam vs lactone norstatine type protease HIV inhibitors: binding energy calculations and DFT study. *J. Biomed. Sci.* **2015**, *22* (1), 15.
(59) Ahmed, M. N.; Yasin, K. A.; Hameed, S.; Ayub, K.; Haq, I.-u.; Tahir, M. N.; Mahmood, T. J. J. o. M. S. Synthesis, structural studies and biological activities of three new 2-(pentadecylthio)-5-aryl-1, 3, 4-oxadiazoles. *J. Mol. Struct.* **2017**, *1129*, 50−59.
(60) Ajeel, F. N.; Khudhair, A. M.; Mohammed, A. A. Research, Density functional theory investigation of the physical properties of dicyano pyridazine molecules. *Int. J. Sci. Res.* **2015**, *4* (4), 2334−2339.
(61) Abbaz, T.; Amel, B.; Villemin, D. Density functional theory studies on molecular structure and electronic properties of sulfanilamide, sulfathiazole, E7070 and furosemide molecules. *J. Appl. Chem.* **2019**, *12*, 60−69.
(62) Horchani, M.; Hajlaoui, A.; Harrath, A. H.; Mansour, L.; Ben Jannet, H.; Romdhane, A. J. J. o. M. S. New pyrazolo-triazolo-pyrimidine derivatives as antibacterial agents: Design and synthesis, molecular docking and DFT studies. *J. Mol. Struct.* **2020**, *1199*, 127007.
(63) Bendjeddou, A.; Abbaz, T.; Gouasmia, A.; Villemin, D. J. I. R. J. o. P.; Chemistry, A. Molecular structure, HOMO-LUMO, MEP and Fukui function analysis of some TTF-donor substituted molecules using DFT (B3LYP) calculations. *Int. Res. J. Pure Appl. Chem.* **2016**, *12* (1), 1−9.
(64) Ahmad, S.; Khan, M. F.; Parvez, S.; Akhtar, M.; Raisuddin, S. Molecular docking reveals the potential of phthalate esters to inhibit the enzymes of the glucocorticoid biosynthesis pathway. *J. Appl. Toxicol.* **2017**, *37* (3), 265−277.
(65) Vijayakumar, V.; Prabakaran, A.; Radhakrishnan, N.; Muthu, S.; Rameshkumar, C.; Isac Paulraj, E. Synthesis, characterization, spectroscopic studies, DFT and molecular docking analysis of N, N′-dibutyl-3, 3′-diaminobenzidine. *J. Mol. Struct.* **2019**, *1179*, 325−335.
(66) Yu, Q.; Fan, L.; Duan, Z. Five individual polyphenols as tyrosinase inhibitors: Inhibitory activity, synergistic effect, action mechanism, and molecular docking. *Food Chem.* **2019**, *297*, 124910.
(67) Kambia, N.; Farce, A.; Belarbi, K.; Gressier, B.; Luyckx, M.; Chavatte, P.; Dine, T. Docking study: PPARs interaction with the selected alternative plasticizers to di (2-ethylhexyl) phthalate. *J. Enzyme Inhib. Med. Chem.* **2016**, *31* (3), 448−455.
(68) Acharya, R.; Chacko, S.; Bose, P.; Lapenna, A.; Pattanayak, S. P. J. S. r. Structure based multitargeted molecular docking analysis of selected furanocoumarins against breast cancer. *Sci. Rep.* **2019**, *9* (1), 15743.
(69) Dai, T.; Li, R.; Liu, C.; Liu, W.; Li, T.; Chen, J.; Kharat, M.; McClements, D. Effect of rice glutelin-resveratrol interactions on the formation and stability of emulsions: A multiphotonic spectroscopy and molecular docking study. *Food Hydrocolloids* **2019**, *97*, 105234.
(70) Santra, D.; Maiti, S. Molecular dynamic simulation suggests stronger interaction of Omicron-spike with ACE2 than wild but weaker than Delta SARS-CoV-2 can be blocked by engineered S1-RBD fraction. *Struct. Chem.* **2022**, *33* (5), 1755−1769.
(71) Ghosh, P.; Bhakta, S.; Bhattacharya, M.; Sharma, A. R.; Sharma, G.; Lee, S.-S.; Chakraborty, C. A novel multi-epitopic peptide vaccine candidate against Helicobacter pylori: in-silico identification, design, cloning and validation through molecular dynamics. *Int. J. Pept. Res. Ther.* **2021**, *27*, 1149−1166.
(72) Zheng, G.; Hussain, Z.; Hayat, C.; Shahab, M.; Sikandar, R.; Bibi, H.; Kamil, A.; Liang, C. Immunoinformatics and Reverse Vaccinology Driven Predication of a Multi-Epitope Vaccine Against Borrelia burgdorferi and Validation Through in silico Cloning and Immune Simulation. *Curr. Pharm. Des.* **2023**, *29*, 1504−1515.


https://doi.org/10.1021/acsomega.3c03342
*ACS Omega* 2023, 8, 32677−32689